Turbulent entrainment in buoyant releases from horizontal gravity current to vertical planar wall plume

Safir Haddad, Samuel Vaux, Kevin Varrall, Olivier Vauquelin

Highlights

Turbulent entrainment in buoyant releases from horizontal gravity current to vertical planar wall plume

Safir Haddad, Samuel Vaux, Kevin Varrall, Olivier Vauquelin

- Study of the evolution of a two-dimensional, turbulent, miscible and steady gravity current and observation of the evolution of the layer using large-eddy simulations, with slopes varying from 0 to 90 degrees.
- The simulations showed three flow regimes. A regime for low angles in which the fluid transitions from the supercritical state to the critical state, a regime for intermediate angles associated with a fluid that remains inertial over its entire length and a regime for high angles in which the flow gains in inertia from the injection.
- In addition, a study of the entrainment for the each slopes revealed an increase with the slope until it reaches a constant value for a slope of 90 degrees, in accordance with the literature.
- Extension of the steady gravity current model introduced by Ellison & Turner (1959) for a non-Boussinesq configuration and highlighting of two specific theoretical angles: the critical angle θ_c, from which the mathematical singularity no longer appears, and the supercritical angle θ_{sc}, from which the fluid gains in inertia as soon as it is injected. These angles are associated with the different regimes observed in the numerical simulations.
- Development of a new entrainment law, including both the slope and the Richardson number, and comparison of the proposed law with those already in existence. In all the configurations discussed, the new law provides more reliable results than those found in the literature.

Turbulent entrainment in buoyant releases from horizontal gravity current to vertical planar wall plume

Safir Haddad[a,b], Samuel Vaux[b], Kevin Varrall[a], Olivier Vauquelin[a]

[a]*Aix-Marseille Université, Laboratoire IUSTI, CNRS UMR 7343, 5 Rue Enrico Fermi, Marseille, 13453, France*
[b]*Institut de Radioprotection et de Sûreté Nucléaire (IRSN), PSN-RES, SA2I, LIE, Centre de Cadarache, Saint-Paul-Lèz-Durance, 13115, France*

Abstract

This paper examines the dynamics of a steady, miscible, two-dimensional gravity current flowing along an inclined boundary, with a particular focus on the entrainment, which refers to the mixing between the gravity current and the surrounding fluid. Specifically, the study investigates the combined effects of the Richardson number Ri and slope θ on the entrainment coefficient E. To address these objectives, large-eddy simulations (LES) were conducted, varying the slope angle from 0° to 90°, while maintaining constant injection conditions.

The simulations revealed three distinct flow regimes for our source conditions. The first regime, observed at low slopes ($\theta < 5°$), exhibits a non-monotonic behavior, characterized by a transition from a supercritical to a subcritical regime. The second regime occurs at intermediate slopes ($5° < \theta < 35°$), where the flow remains inertial throughout. In the third regime, associated with steeper slopes ($\theta > 35°$), the flow immediately gains inertia upon injection. The simulations also enabled an analysis of E, which was found to increase with slope and reach a constant value at $\theta = 90°$.

A theoretical investigation of gravity currents was also conducted, resulting in the extension of the theoretical model of Ellison & Turner (1959) in the non-Boussinesq configuration as well as the identification of two specific angles: the critical angle θ_c, beyond which no mathematical singularity occurs, and the supercritical angle θ_{sc}, above which the flow acquires inertia immediately after injection.

Moreover, a new entrainment law was developed, incorporating both the effects of the Richardson number and the slope: $E = 0.002\cos(\theta)/\mathrm{Ri} + 0.09\sin^{1/2}(\theta)$. This law provides a description of the entrainment behavior across the full range of slope angles. Comparisons between the LES results and the theoretical model demonstrate that the proposed entrainment law offers improved accuracy over existing models for all slope configurations, including the extreme cases of gravity currents ($\theta = 0°$) and planar wall plumes ($\theta = 90°$).

Keywords: gravity current, entrainment, slope, non-Boussinesq

1. Introduction

A gravity current is a flow driven horizontally by a difference between its own density and the density of its surroundings. This difference may result from distinct mechanisms such as a variation in temperature, salinity or concentration. The comprehension of this family of flows is of paramount importance for a better understanding of natural (Griffiths (1986), Dufek (2016))

or industrial (Hoult (1972)) processes. Typically, gravity currents propagate along a boundary, which may be inclined or horizontal. Alternatively, it can develop between two layers of fluids of different densities. In this configuration, which will not be discussed in the present paper, the current is known as an intrusion (Flynn & Linden (2006)).

Gravity currents are complex flows and are commonly studied for two configurations. The first configuration, known as the "lock-exchange", involves an initially fixed volume of fluid being released into an environment of different density (Shin et al. (2004)). This unsteady set-up allows the investigation of several phenomena such as the velocity of the front (Rottman & Simpson (1983)) or the influence of the wall on the propagation (Nogueira et al. (2013)).

The second configuration corresponds to a continuous release of the current from a nozzle. In this set-up, the unsteady state of the flow can also be studied. For example, Hogg & Woods (2001) work on the influence of the drag on the propagation velocity, Sher & Woods (2017) deal with the entrainment of the head and Martin et al. (2020) study the influence of the slope. In contrast to the lock-exchange setup, this configuration enables the observation of a steady-state, enabling to model the flow using "top-hat" variables, akin to the models developed for plumes by Morton et al. (1956) and for gravity currents by Ellison & Turner (1959).

In their pioneering work, these latter authors proposed a theoretical model based on the conservation equations for mass, momentum, and energy. This theoretical model yields a system of coupled ordinary differential equations, which describe the streamwise evolution of the top-hat velocity U, the top-hat density ρ and the thickness h of the current. These equations introduce the Richardson number, corresponding to the ratio between the buoyancy and inertia forces, and defined as follows : $\mathrm{Ri} = \Delta\rho\, g\, h \,/\, \rho_a\, U^2$ (with $\Delta\rho = |\rho - \rho_a|$, ρ_a being the density of the ambient and g the gravitational acceleration). The Richardson number is also used to characterize the flow by defining three regimes: supercritical when $\mathrm{Ri} < 1$ (momentum-dominated), sub-critical when $\mathrm{Ri} > 1$ (buoyancy-dominated) and critical when $\mathrm{Ri} = 1$.

Inherent in their model, Ellison & Turner (1959) particularly address the issue of local entrainment. This phenomenon, which occurs when fluids are miscible, corresponds to the mixing between the fluid and its environment. Using a small-scale experiment, these authors identified a dependency between the Richardson number and the entrainment coefficient E expressed as $E \propto \mathrm{Ri}^{-1}$. Furthermore, Ellison & Turner (1959) suggest that entrainment becomes negligible when $\mathrm{Ri} > 0.8$. Later, Turner (1986) provides the mathematical relation associated with these results:

$$E = \frac{0.08 - 0.1\,\mathrm{Ri}}{1 + 5\,\mathrm{Ri}} \quad \text{for} \quad \mathrm{Ri} < 0.8. \tag{1}$$

The work of Ellison & Turner (1959) became the foundation for many subsequent studies, partially compiled in Fernando (1991), which were aimed at refining the modelling of the local entrainment coefficient E. The majority of these works support the relation between the Richardson number and the entrainment coefficient initially proposed by Ellison & Turner (1959) (Parker et al. (1986), Johnson & Hogg (2013)). However, some researchers argue that entrainment persists even when the Richardson number exceeds unity (Lofquist (1960), Princevac et al. (2005)), while others contend that a single governing law cannot describe the entire range of Richardson numbers (Christodoulou (1986)). Additionally, certain models incorporate further parameters, such as a flux coefficient (Wells & Wettlaufer (2005)) or the Reynolds number (Cenedese & Adduce (2010)).

The study by Ellison & Turner (1959) also covers the entrainment with a slope of 90° (similar to a planar wall plume bounded by a vertical surface). In this configuration, the authors use a

global entrainment coefficient E_{global} calculated from the difference between the inlet and outlet mass flow rates to quantify the amount of fluid entrained. Ellison & Turner (1959) obtained a constant entrainment coefficient equal to $E_{\text{global}} = 0.087$. They report that this result is in agreement with the value of 0.075 observed for a jet, while being in the same range as the result provided by Morton et al. (1956) in their seminal work on the modeling of an axisymmetric plume ($E = 0.1$).

In the specific case where the slope angle is 90°, Grella & Faeth (1975) conducted experiments that included the effects of heat transfer to investigate the influence of the wall on local entrainment. They found $E = 0.095$, which closely matches the value recently found by Zúñiga et al. (2024) through direct numerical simulations (DNS). The magnitude of these findings is further supported by the freshwater/saltwater experiments conducted by Parker et al. (2020), where $E = 0.08$. Additional experimental investigations (Lai & Faeth (1987), Sangras et al. (2000)) and DNS simulations (Georges et al. (2021)) corroborate these results, suggesting that the entrainment coefficient for a top-hat planar wall plume (or gravity current inclined at 90°) is close to 0.09.

Finally, Ellison & Turner (1959) also reported results for global entrainment at varying slope angles. The authors observe an increase in entrainment with increasing inclination. The subsequent literature provides less detail on the inclined configuration. Britter & Linden (1980), from visual observations, present quantitative values of the entrainment with a slope. Although direct comparison with the data from Ellison & Turner (1959) was not possible due to differences in post-processing methods (Ellison & Turner (1959) is based on the top-hat height and Britter & Linden (1980) is based on the visual thickness of the flow), the trend of increased entrainment with slope was confirmed. Pawlak & Armi (2000), on their side, found significantly larger entrainment values than those reported by Ellison & Turner (1959) for slopes less than 15°. Zúñiga et al. (2024) also dealt with this issue by performing DNS simulations at different angles. They observed a thickening of the current, and came to the same conclusions as Ellison & Turner (1959), with an increase in entrainment as the slope increases, until it becomes constant for steep slopes ($\theta > 61°$). Several other authors have proposed angle-dependent entrainment laws, which are summarized in table 1.

The majority of these laws are solely dependent on the slope angle, assuming a constant entrainment coefficient for a given angle regardless of the Richardson number. This is in agreement with the literature for angles near 90°. However, for smaller angles, the influence of the

Reference	Law	Remarks
Pedersen (1980)	$0.072 \sin(\theta)$	-
Briggs (1980)	$0.05 \sin(\theta)^{2/3}$	-
Hopfinger (1983)	$9.5 \times 10^{-4}(\theta + 5)$	Law based on Ellison & Turner (1959)
Hopfinger (1983)	$4 \times 10^{-3}\theta$	Law based on Britter & Linden (1980)
Wells & Wettlaufer (2005)	$E_p \sin(\theta)$	$\theta > 5°$
Hughes & Griffiths (2006)	$0.1 \sin(\theta)$	$\theta > 5°$
Salinas et al. (2022)	$\frac{\text{Ri}\tan(\theta) - C_d}{C}$	$0.14° < \theta < 2.86°$

Table 1: Entrainment laws from the literature including an angle.

Richardson number on the entrainment could be questioned. The only law combining these two parameters is the one suggested by Salinas et al. (2022), but it is restricted to very low slopes ($0.14° < \theta < 2.86°$).

The question that now arises, and which we will attempt to answer throughout this paper, is the following: Is it possible to establish an entrainment law that accounts for both the Richardson number and slope angle in order to respect the observations made in the literature for slopes varying between 0° and 90° ? Such a law requires us to observe the local evolution of the current, in contrast to the law given by Ellison & Turner (1959), which is based exclusively on global quantities.

To answer this question, our investigation proceeds in several stages. Firstly, to investigate the physics of these flows, section 2 describes the large-eddy simulations carried out for slopes ranging from 0 to 90°. These simulations are then post-processed to extract local information on the top-hat variables as well as the entrainment. In section 3, the theoretical aspects of the current are studied, in particular the influence of slope on the equations, and we develop a new entrainment model based both on the simulation results and the literature. This entrainment model is then challenged in section 4 before finally drawing conclusions in the last section of the paper.

2. Numerical simulations

To simulate a non-Boussinesq turbulent miscible gravity current, we consider an isothermal and continuous release of an air-helium mixture along an inclined boundary within a denser ambient environment. In the set of eight simulations carried out, the velocity and the density of the flow at the source are fixed at $u_0 = 1.3\,\mathrm{m/s}$ and $\rho_0 = 1\,\mathrm{kg/m^3}$, respectively. The source height remains constant either and is set to $h_0 = 0.2\,\mathrm{m}$. The ratio between the density of the injected fluid and the ambient fluid is $\rho_0/\rho_a = 0.914$ (weakly non-Boussinesq). Under these source conditions, the Richardson and Reynolds ($\mathrm{Re}_0 = u_0 h_0/\nu$, where ν is the kinematic viscosity) numbers are respectively 0.237 and 14 000. The only variable parameter is the tilt angle θ, and the set of simulations performed is shown in table 2.

We use large-eddy simulations (LES) to solve the Favre-filtered mass and momentum balance, using the numerical computational code CALIF^{3}S. This software, developed at the French

	u_0 (m/s)	$\rho_0\left(\mathrm{kg/m^3}\right)$	h_0 (m)	Ri_0	Re_0	θ (°)	L (m)
Case 0	1.3	1	0.2	0.237	14 000	0	9
Case 1	1.3	1	0.2	0.237	14 000	5	9
Case 2	1.3	1	0.2	0.237	14 000	11	9
Case 3	1.3	1	0.2	0.237	14 000	19	9
Case 4	1.3	1	0.2	0.237	14 000	35	9
Case 5	1.3	1	0.2	0.237	14 000	56	9
Case 6	1.3	1	0.2	0.237	14 000	77	9
Case 7	1.3	1	0.2	0.237	14 000	90	9

Table 2: Source conditions, Richardson number, Reynolds number, slope angle, and length of the domain of the simulations carried out.

Institut de Radioprotection et de Sûreté Nucléaire (IRSN), is specifically designed for three-dimensional simulations of turbulent and slightly compressible flows. The three-dimensional (index i) filtered Navier-Stokes equations are:

$$\frac{\partial \overline{\rho}}{\partial t} + \frac{\partial (\overline{\rho}\widetilde{u_i})}{\partial x_i} = 0, \tag{2}$$

$$\frac{\partial (\overline{\rho}\widetilde{u_i})}{\partial t} + \frac{\partial (\overline{\rho}\widetilde{u_i}\widetilde{u_j})}{\partial x_j} = -\frac{\partial \overline{p}}{\partial x_i} + \frac{\partial \overline{S}_{ij}}{\partial x_j} + (\rho_a - \overline{\rho})\, g_\theta - \frac{\partial \tau_{ij}}{\partial x_j}, \tag{3}$$

where $\widetilde{u_i}$ represents the Favre-filtered velocity and $\overline{p}$ denotes the dynamic pressure. $\overline{\rho}$ is the filtered density of the fluid and is computed using the ideal gas law and the mass fractions of the different species in the gas mixture. In equation (3), $g_\theta = g\cos(\theta)$ correspond to the gravitational acceleration, $\tau_{ij} = \overline{\rho u_i u_j} - \overline{\rho}\widetilde{u_i}\widetilde{u_j}$ is the subgrid-scale Reynolds stress, and $\overline{S}_{ij} = -(2/3)\,\mu(\partial\widetilde{u_k}/\partial x_k)\delta_{ij} + \mu\,(\partial\widetilde{u_i}/\partial x_j + \partial\widetilde{u_j}/\partial x_i)$ represents the filtered strain rate tensor and μ is the dynamic molecular viscosity.

The mass fraction y_k for each species k is determined through the transport equation for species:

$$\frac{\partial \overline{\rho}\widetilde{y_k}}{\partial t} + \frac{\partial (\overline{\rho}\widetilde{y_k}\widetilde{u_i})}{\partial x_i} = \frac{\partial}{\partial x_i}\left(\overline{\rho} D\, \frac{\partial \widetilde{y_k}}{\partial x_i} + \frac{\mu_t}{Sc_t}\frac{\partial \widetilde{y_k}}{\partial x_i}\right), \tag{4}$$

where $\widetilde{y_k}$ is the Favre-filtered mass fraction of the k-th component of the mixture, and D is the molecular diffusivity of the mixture. The closure of the problem is achieved by setting the turbulent Schmidt number Sc_t to 0.7, following the simple gradient diffusion hypothesis (SGDH). The code has already been used and validated to study flows characterised by small or large density differences, such as gravity currents (Haddad et al. (2022)), heavy and light discharges such as jets (Salizzoni et al. (2023), Salizzoni et al. (2024)) and fountains (Vaux et al. (2019)).

In our large-eddy simulations, we adopt the wall adapting local eddy subgrid-scale model (WALE, Nicoud & Ducros (1999)) for the subgrid Reynolds stress and we apply a box filter in each direction. A staggered grid with a cell-centred piecewise constant representation of the scalar variables is used as well as a marker and cell (MAC) type finite volume approximation for the velocity. The time discretization is done with a fractional step algorithm decoupling balance equations for the transport of species and Navier-Stokes equations. These latter are solved by a pressure correction technique.

The computational domain Ω is a rectangular box of dimensions $L_x \times L_y \times L_z$. The horizontal length is $L_x = L_0 + L$ (where L_0 is the position of the injection and is equal to $5h_0$). The vertical length L_z is equal to $20h_0$ and the spanwise width L_y is equal to $6h_0$.

In the horizontal streamwise direction of Ω, the mesh is divided into two zones: the first extends from $x = 0$ to the injection position $x_i = L_0$ and the second from the injection position to the outlet position at L_x. In the first zone, a uniform Cartesian rectangular mesh ($\Delta x_1 \times \Delta y$) is used. The grid is refined in the second zone with a uniform rectangular mesh ($\Delta x_2 \times \Delta y$).

In the vertical direction (z), the grid spacing Δz is kept constant from the ceiling to the injection height i.e. $z = h_0$ (with $\Delta z = \Delta z_1$), still uniform from $z = h_0$ up to a vertical distance L_{1z} corresponding approximately to the boundary of the current. Beyond this region, the grid is further stretched until it reaches the bottom of the domain.

For each case, we performed a grid-convergence study to validate the extent of the vertical subregion L_{1z} and the grid resolution in each direction. We tested vertical grid spacings $\Delta z_1/h_0$ ranging from 0.1 to 0.05 and $\Delta z_2/h_0$ ranging from 0.15 to 0.075, horizontal grid spacings $\Delta x_1/h_0$

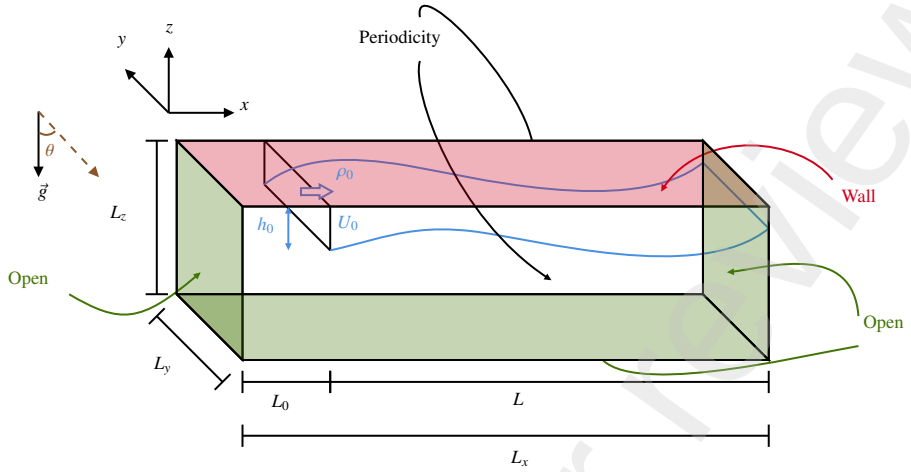

Figure 1: Representation of the computational domain Ω with the boundary conditions associated to the border of this domain.

from 0.15 to 0.075 and $\Delta x_2/h_0$ from 0.1 to 0.06 and finally spanwise grid spacing $Deltay/h_0$ from 0.15 to 0.05. For the time discretization, we impose a Courant-Friedrichs-Lewy number close to unity even if time step sizes for which CFL numbers greater than one are allowed with implicit schemes.

Given that the modeled flow propagates in an infinite (open) environment, it is necessary to bound the computational domain Ω with artificial boundary conditions, as illustrated in figure 1. For the left, bottom and right boundaries, we apply a boundary condition based on the usual control of the kinetic energy, which allows us to distinguish between the flow that enters the domain and the flow that leaves. This type of condition was originally formulated for incompressible flows in Bruneau & Fabrie (1994) and in Bruneau & Fabrie (1996), and its extension to compressible flows was tackled in Bruneau (2000). In addition, periodic boundary conditions are imposed in the spanwise direction. Finally, the flow emerges horizontally from the source with a uniform velocity profile, and the turbulence at the source is triggered by azimuthal forcing, following the approach of Zhou et al. (2001).

Since the study focuses on steady-state flow, the simulation duration is set sufficiently long to ensure convergence of the time-averaged statistics of the flow variables. The steady state is considered to be achieved when the variation in the mean statistical values falls below 2% of the mean value.

Finally, the cross-section scales of the velocity, thickness and density (respectively denoted $U(x)$, $h(x)$ and $\rho(x)$) are obtained using the following integral formulations for the mass, volume

and momentum fluxes per unit depth (Ellison & Turner (1959)):

$$\rho(x)\, U(x)\, h(x) = \int_0^\infty \varrho(x,z)\, u(x,z) \mathrm{d}z, \tag{5}$$

$$U(x)\, h(x) = \int_0^\infty u(x,z) \mathrm{d}z, \tag{6}$$

$$\rho(x)\, U(x)^2\, h(x) = \int_0^\infty \varrho(x,z)\, u(x,z)^2 \mathrm{d}z, \tag{7}$$

where $u(x,z)$ and $\varrho(x,z)$ represent the local velocity and density of the layer, respectively. For the sake of clarity, in the following, $\rho(x)$, $U(x)$ and $h(x)$ will be referred to simply as ρ, U and h respectively.

2.1. Longitudinal evolution of the current

Before examining the influence of slope on the entrainment, we first focus on the longitudinal evolution of the variables U, h and ρ, defined in the previous paragraph with the equations (5), (6) and (7), along with the Richardson number Ri for the eight cases simulated. Figure 2 shows these longitudinal evolutions for the eight cases.

For the case 0 ($\theta = 0°$, blue lines with squares in figure 2), the simulation shows a transition. Specifically, both height and Richardson number increase until reaching a maximum at $x = 2.3$m

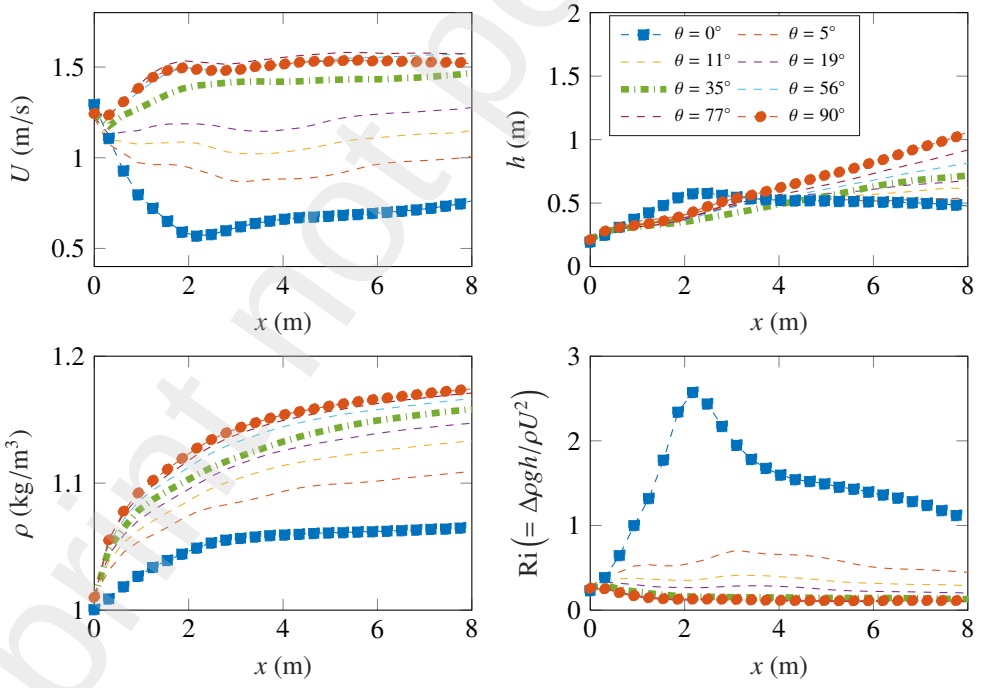

Figure 2: Longitudinal evolution of the velocity, the height, the density and the Richardson number of the flow for all the cases presented in table 2.

after which they decrease until the exit of the domain. The velocity also exhibits this non-monotonic behavior with first a decrease and then an increase. Moreover, a transition from the supercritical to the subcritical regime is observed as the Richardson number exceeds unity.

As the slope angle increases and reaches 5°, we notice that the Richardson number of the flow does not reach unity. This indicates that there is therefore no transition associated to a change of regime, although a slight non-monotonic behaviour is observed. Regarding velocity and height, the former decreases initially and then stabilizes, while the latter increases continuously from the injection point to the domain exit. This general behavior is consistent for all simulations with slope angles below 35° (i.e. slope of 11° and 19°).

For angles equal or greater than 35° (green dashdotted lines in figure 2), a different behavior is observed. Although the velocity decreases near the injection point, it increases rapidly and stabilizes around $x = 2\,\mathrm{m}$ until reaching the exit. This change, also reflected in the Richardson number, suggests a new behavior where the flow gains inertia shortly after injection. These findings are consistent with the observations of Baines (2005), who identified a transition between the "gravity current" like and the "plume" like behavior for slopes in the range of $[20°, 30°]$. In addition, for angles equal to or greater than 35°, the thickness of the current evolves linearly, which is typical of plume-like flows (Michaux & Vauquelin (2008)).

Finally, for a 90-degree slope (orange lines with circles in figure 2), the results show that the velocity of the flow increases before reaching a constant value. The Richardson number decreases slightly before stabilizing, and the height increases linearly. Additionally, the density increase is most pronounced in this configuration, indicating that entrainment is greater for this angle than for any of the others.

2.2. Study of the entrainment

In addition to the primary variables U, h, and ρ, the simulations also enable the computation of the local entrainment coefficient E at each longitudinal position x. This coefficient is derived from the mass conservation equation presented in Ellison & Turner (1959) and rewritten as:

$$E(x) = \frac{\mathrm{d}\left(\rho\, U\, h\right)}{\mathrm{d}x}\,\frac{1}{U\,\rho_a}, \tag{8}$$

From the relation (8), the evolution of the local entrainment as a function of the Richardson number can be plotted, as shown in figure 3. Note that we have chosen to disregard data close to the injection point ($x < 3\,\mathrm{m}$) and the outlet ($x > 7\,\mathrm{m}$) to avoid any potential influence of the boundary conditions on the entrainment.

The analysis of figure 3 reveals, first and foremost, that the entrainment coefficient increases with the slope. Specifically, each successive angle exhibits a higher entrainment than the preceding one. Additionally, for steeper angles (77° and 90°), the entrainment appears to remain relatively constant, with values approaching 0.09, which is consistent with the value mentioned in the introduction for a vertical planar wall plume.

Moreover, this figure shows that the entrainment becomes progressively more constant as the slope increases. Finally, this figure also shows that the influence of angle strongly depends on the magnitude of the angle. For small slope angles, the increase in entrainment seems to be slight, whereas for larger angles, this increase is more pronounced.

These results confirm that entrainment is influenced by both the Richardson number and the slope. At lower slope angles, the Richardson number plays a significant role, but its influence

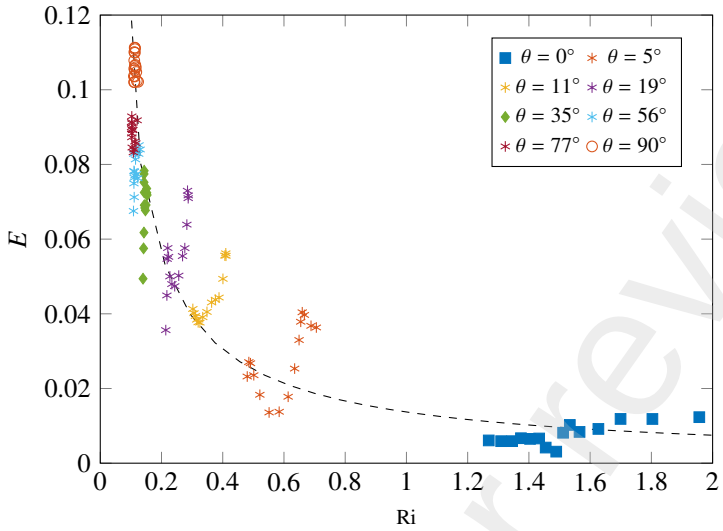

Figure 3: Evolution of the local entrainment E as a function of the Richardson number Ri for all the cases presented in table 2.

diminishes as the slope increases, eventually vanishing for vertical angles (90°). It is now interesting to focus on the theoretical aspects of the current in order to better understand the influence of the slope on the flow.

3. Theory

3.1. Governing equations

We consider a steady gravity current flowing along a wall of length L, inclined at an angle θ to the horizontal, as illustrated in figure 4. The current is released with a density ρ_0 at a horizontal velocity u_0 from a rectangular nozzle of thickness h_0. The surrounding fluid, having a density ρ_a ($> \rho_0$), is at rest. Furthermore, we assume that the flow is always supercritical at the injection, as in the simulations carried out in section 2 (i.e. $\mathrm{Ri}_0 < 1$). The cross-section scales of the velocity, thickness and density, denoted by U, h and ρ, respectively, are obtained using the integral formulations for the mass, volume and momentum fluxes presented in equations (5), (6) and (7).

The governing equations of the steady gravity current are derived by considering a balance of mass, momentum and buoyancy on an infinitesimal element of length dx. These governing equations can be expressed as follows:

$$\frac{\mathrm{d}\left(\rho\, U\, h\right)}{\mathrm{d}x} = E\, U\, \rho_a, \tag{9}$$

$$\frac{\mathrm{d}\left(\rho\, U^2\, h\right)}{\mathrm{d}x} = \Delta\rho\, g\, h \sin(\theta) - \frac{1}{2}\frac{\mathrm{d}\left(\Delta\rho\, g\, h^2\, \cos\theta\right)}{\mathrm{d}x} - C_d\, \rho\, U^2, \tag{10}$$

$$\frac{\mathrm{d}}{\mathrm{d}x}\left(\frac{\Delta\rho}{\rho_a}\, g\, U\, h\right) = 0, \tag{11}$$

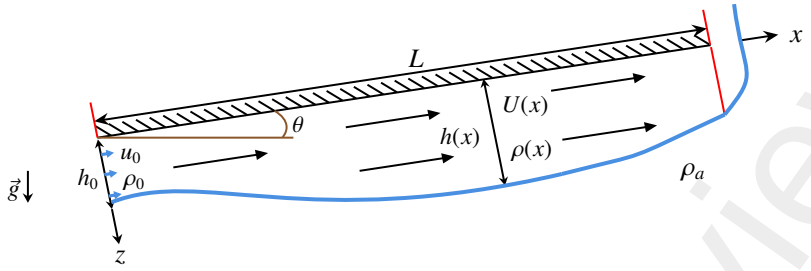

Figure 4: Schematic of the inclined gravity current configuration.

where E is the local entrainment coefficient and C_d represents the drag coefficient. The RHS of the equation (10) stand respectively for the buoyancy force due to the slope, the pressure force on the flow arising from variations in thickness and density and the basal drag force due to the friction between the current and the inclined wall. These ordinary differential equations can be combined to derive the longitudinal evolution of the velocity, thickness and density:

$$\frac{\mathrm{d}\,U}{\mathrm{d}x} = -\frac{U}{h}\frac{\left(\frac{\rho_a}{\rho} - \frac{1}{2}\,\mathrm{Ri}_\theta\right)E + C_d - \mathrm{Ri}_\theta\,\tan\theta}{1 - \mathrm{Ri}_\theta}, \tag{12}$$

$$\frac{\mathrm{d}\,h}{\mathrm{d}x} = \frac{\left(1 + \frac{\rho_a}{\rho} - \frac{1}{2}\,\mathrm{Ri}_\theta\right)E + C_d - \mathrm{Ri}_\theta\,\tan\theta}{1 - \mathrm{Ri}_\theta}, \tag{13}$$

$$\frac{\mathrm{d}\,\rho}{\mathrm{d}x} = \frac{\Delta\rho\,E}{h}, \tag{14}$$

where Ri_θ is the projected Richardson number:

$$\mathrm{Ri}_\theta = \frac{\Delta\rho\,h\,g\cos\theta}{\rho\,U^2} = \mathrm{Ri}\cos\theta. \tag{15}$$

The evolution of Ri_θ is obtained by combining equations (12), (13), (14) and (15):

$$\frac{\mathrm{d}\,\mathrm{Ri}_\theta}{\mathrm{d}x} = \frac{\mathrm{Ri}_\theta}{h}\frac{\left(1 + 2\,\frac{\rho_a}{\rho}\right)\left(1 + \frac{1}{2}\,\mathrm{Ri}_\theta\right)E + 3\,C_d - 3\,\mathrm{Ri}_\theta\,\tan\theta}{1 - \mathrm{Ri}_\theta}. \tag{16}$$

When the angle tends towards 0 in equations (12), (13), (14) and (16), we find the equations for a non-Boussinesq gravity current propagating on a horizontal wall. In this configuration, the Richardson number increases until it reaches unity, where a singularity arises. Haddad et al. (2024) proposed to introduce a discontinuity, similar to a hydraulic jump, to circumvent this issue. The location and amplitude of this jump are determined using conservation equations on either side of the discontinuity, as well as a critical boundary condition at the exit of the domain. However, as the slope increases, the mathematical singularity no longer appears. Indeed, a closer look at equations (12), (13) and (16) reveals that when the following condition is met:

$$\theta > \arctan\left[\frac{\left(1 + 2\,\frac{\rho_a}{\rho}\right)(1 + 2\,\mathrm{Ri}_\theta)\;E + 3\,C_d}{3\,\mathrm{Ri}_\theta}\right], \tag{17}$$

then the numerator of equations (12), (13) and (16) is not strictly positive. By replacing Ri_θ by 1, it is possible to define the critical angle θ_c:

$$\theta_\mathrm{c} = \arctan\left[\left(1 + 2\,\frac{\rho_a}{\rho}\right) E + C_d\right], \tag{18}$$

which corresponds to the angle beyond which the singularity is never reached. Additionally, if the slope angle exceeds this critical angle, the numerator of (16) becomes zero before Ri_θ reaches unity. In this case, the flow reaches a "normal regime", as Ellison & Turner (1959) called it in their article, in which the Richardson number no longer varies. Conversely, if the slope is less than this critical angle, the mathematical singularity arises. Practically, although it depends on the ratio between the densities as well as the entrainment and drag coefficients, this angle is quite small, as specified by Britter & Linden (1980) who experimentally obtained $\theta_\mathrm{c} = 0.5°$. These findings are corroborated by the results of the LES simulations presented in section 2, where it was observed that for a 5° slope, the Richardson number no longer reaches unity and tends towards a constant value, indicating that the critical angle θ_c has been exceeded, for our source conditions.

Moreover, we can investigate the angle from which the normal state is achieved immediately after the injection. Referring to equation (17), and substituting Ri_θ by $\mathrm{Ri}_\theta(x = 0)$, we then find the supercritical angle θ_sc:

$$\theta_\mathrm{sc} = \arctan\left[\frac{\left(1 + 2\frac{\rho_a}{\rho}\right)(1 + 2\,\mathrm{Ri}_\theta(x=0))\; E + 3\,C_d}{3\,\mathrm{Ri}_\theta(x=0)}\right]. \tag{19}$$

When $\theta > \theta_\mathrm{sc}$, the fluid gains in inertia and the Richardson number decreases immediately after the injection. When $\theta = \theta_\mathrm{sc}$, the Richardson number remains constant from the injection to the exit of the domain. Finally, for $\theta_\mathrm{c} < \theta < \theta_\mathrm{sc}$, the Richardson number increases until the fluid reaches the normal state and remains constant. For our source conditions, it was found that the supercritical angle θ_sc appears to be near 35°.

By the way, for the particular case when $\theta = 90°$, namely for the planar wall plume, equations (9), (10) and (11) lead to:

$$\frac{\mathrm{d}\,(\rho\,U\,h)}{\mathrm{d}x} = E\,U\,\rho_a, \tag{20}$$

$$\frac{\mathrm{d}\,(\rho\,U^2\,h)}{\mathrm{d}x} = \Delta\rho\,g\,h - C_d\,\rho\,U^2, \tag{21}$$

$$\frac{\mathrm{d}}{\mathrm{d}x}\left(\frac{\Delta\rho}{\rho_a}\,g\,U\,h\right) = 0. \tag{22}$$

These equations correspond to those presented by Parker et al. (2020) but extended to the non-Boussinesq configuration. For this slope, the entrainment coefficient E is constant (≈ 0.09).

3.2. A generalized entrainment coefficient ?

Given that above observations show that both the Richardson number and the slope angle influence the entrainment, we propose to include these two parameters in a new entrainment law. This model must satisfy three conditions:

- The law depends only on the Richardson number when the slope angle is null.

- The law is constant when the slope angle is 90°.
- The influence of the planar wall plume must be greater than the influence of the gravity current.

On the basis of these considerations and from the results of the literature introduced in section 1, we propose to combine the law of Christodoulou (1986), valid for a range of $\mathrm{Ri} \in [0.1, 10]$, with the observations from the LES simulations and for the vertical planar wall plume in order to write:

$$E(\theta, \mathrm{Ri}) = \frac{0.002}{\mathrm{Ri}} \cos\theta + 0.09 \sin^{1/2}\theta. \tag{23}$$

The coefficient $1/2$ on the sinus term is intended to represent the transition from the gravity flow behaviour to the planar wall plume behaviour mentioned in the third condition above. This is in agreement with the results of Baines (2005), who suggest that the "plume" behaviour manifests before the "gravity current" behaviour disappears.

4. Comparison between the theoretical model and the numerical simulations

We can now test the reliability and robustness of the generalized entrainment model (23) by comparing the results of the LES simulations with those of the theoretical model (equations (12), (13) and (14)). The model requires also a value for the drag coefficient, and we adopt the value $C_d = 0.0065$ as prescribed in Kunsch (1998). This coefficient corresponds to a flow of hot air into an ambient environment and has been used in similar studies, such as Hu et al. (2005), Chow et al. (2015), Chow et al. (2016) and Haddad et al. (2022).

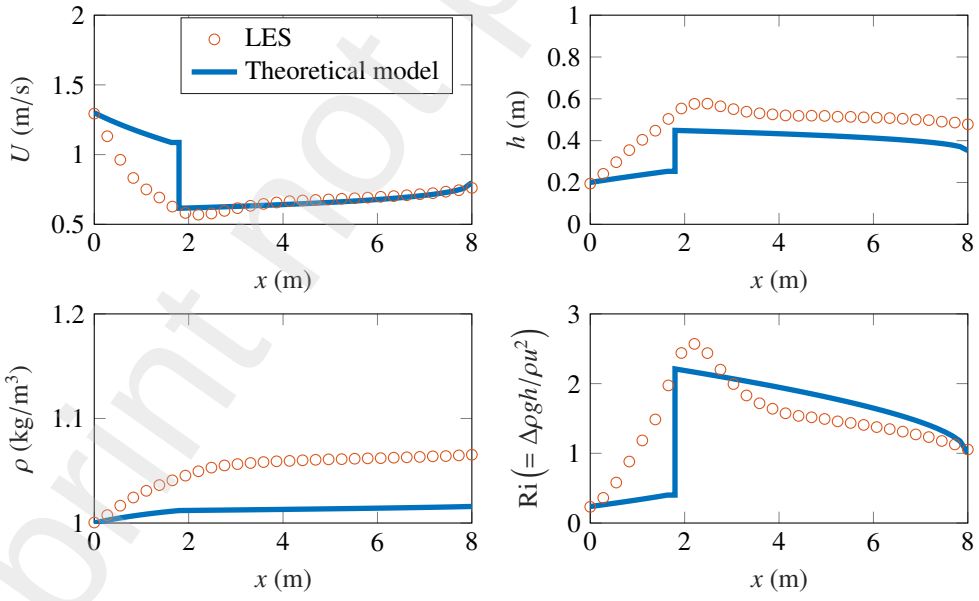

Figure 5: Longitudinal evolution of the velocity, the height, the density and the Richardson number of the flow for the case 0 ($\theta = 0°$). The red circles correspond to LES simulation and the blue lines correspond to the solution given by theoretical model.

In the no-slope configuration (case 0, $\theta = 0°$), a straightforward numerical resolution with the theoretical model is not achievable. As discussed in section 2.1, the flow exhibits non-monotonic behaviour, and the Richardson number exceeds unity, leading to the appearance of a singularity during the solving. To circumvent this issue, we used the hydraulic jump without entrainment. Further details of the solution method can be found in the work of Haddad et al. (2022), but briefly the method consists in applying the Bélanger (or Rankine-Hugoniot) equations before reaching the singularity to jump from a Richardson number below unity to a Richardson number above unity. The location of the jump is then defined by imposing $\mathrm{Ri} = 1$ at the exit of the domain, as in the hydraulic configuration (Henderson (1966), Chanson (2004)). Hence, the solution satisfies the conservation equations for the supercritical phase, the Bélanger equations for the regime transition, the conservation equations for the sub-critical phase (after the jump) and critical Richardson number at the exit of the domain.

Comparisons between the model and the LES simulation for the velocity, the height, the density and the Richardson number of the current are displayed in figure 5. This figure shows that the theoretical model, incorporating the jump, reproduces the non-monotonic behavior of the flow. From a quantitative point of view, the theoretical model provides a reliable estimation of U, h and ρ on both side of the discontinuity, although it slightly underestimates the thickness. The primary source of discrepancy lies in the abrupt nature of the hydraulic jump in the model, which is more gradual in the simulation. Regarding the density, the model exhibits similar behaviour with a relative error of less than 5%, indicating that the selected entrainment law is appropriate for this type of flow.

In the case with a slope, we compare the theoretical results obtained using the entrainment

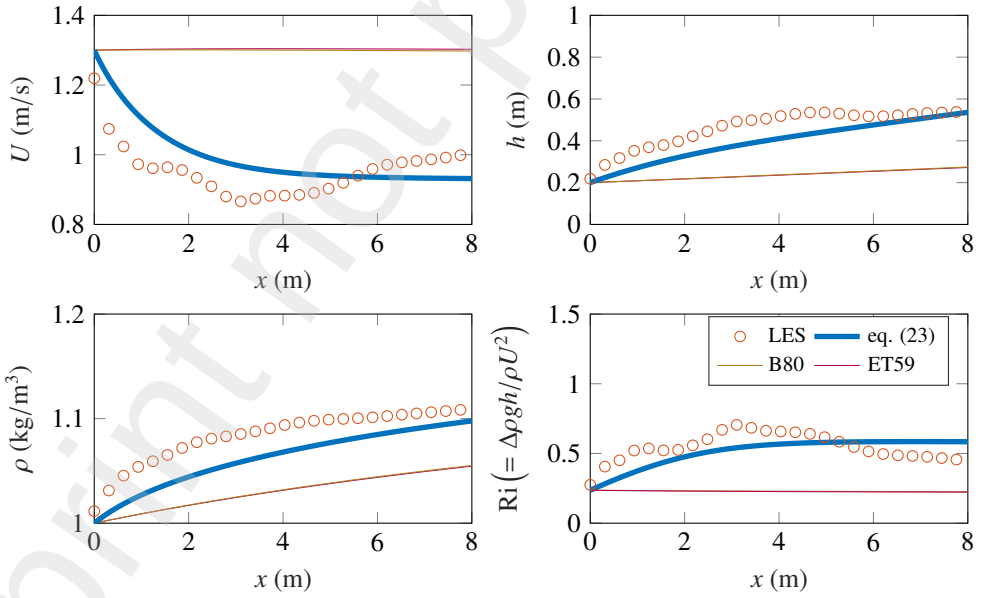

Figure 6: Longitudinal evolution of the velocity, the height, the density and the Richardson number of the flow for the case 1 ($\theta = 5°$). The red circles correspond to the LES simulation. The theoretical results are obtained by successively using the entrainment law given by equation (23) as well as the laws of Hopfinger (1983) based on the results of Ellison & Turner (1959) (ET59) and Briggs (1980) (B80).

law (23) with the theoretical results obtained using the law established by Briggs (1980) (see table 1) and the law of Hopfinger (1983) derived from the data of Ellison & Turner (1959). The results obtained with the LES simulation and with the theoretical model for these different laws on a weak slope (5°) are shown in figure 6. It becomes apparent that the entrainment laws from the literature fail to accurately represent the flow, resulting in relative errors in the primary quantities on the order of 50%. These laws seem inadequate to capture the behavior of the flow with an almost constant velocity and Richardson number on the whole domain, whereas the simulation clearly shows an increase and a decrease, respectively. This suggests that a global approach is not well-suited for modeling such flows under these conditions. On the contrary, when applying the entrainment law given by relation (23), the model provides more accurate results, both qualitatively and quantitatively, for all the variables calculated. This is especially true for the density, which suggests that the entrainment is more conveniently represented by the newly built relation (23). Nevertheless, even if our model cannot reproduce some slight non-monotonic local behaviours observed in the LES simulation (near the injection and the outlet), it gives an acceptable estimation of these quantities over a large section of the domain.

The same graphs can be plotted with an intermediate slope (35°) (figure7). In this case, the entrainment laws from the literature yield better results than in the previous configuration, but the relation (23) provides again better results, with relative errors on height and density of less than 8% and 5%, respectively.

For a steeper slope ($\theta = 77°$), the results are displayed in figure 8. This time, the law of Briggs (1980) provides the least satisfactory results. The law of Hopfinger (1983), based on the results of Ellison & Turner (1959), offers results that are reasonably consistent with the LES simulation, in

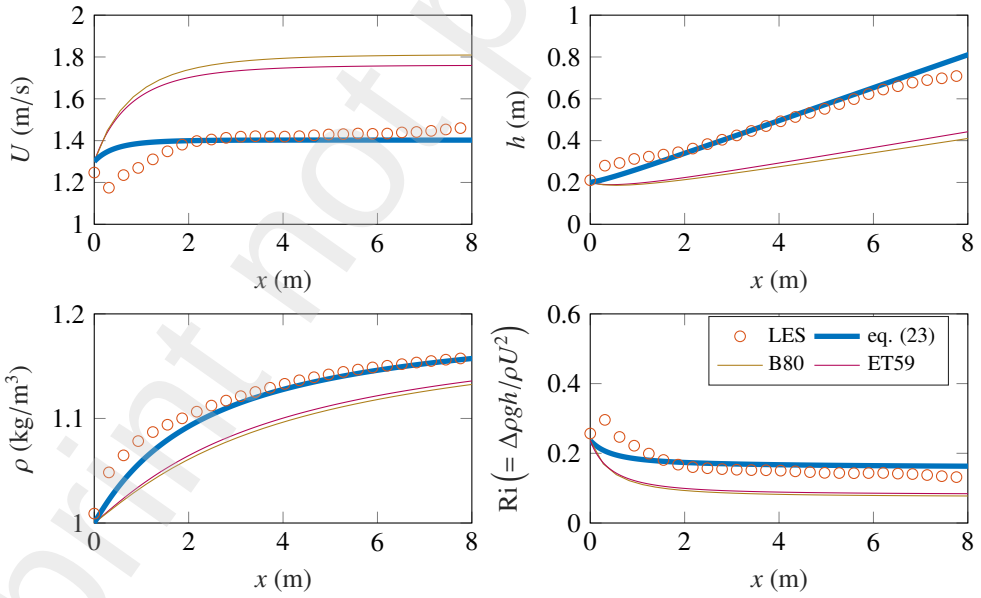

Figure 7: Evolution of the velocity, the height, the density and the Richardson number of the flow for the case 4 ($\theta = 35°$). The red circles correspond to the LES simulation. The theoretical results are obtained by successively using the entrainment law given by equation (23) as well as the laws of Hopfinger (1983) based on the results of Ellison & Turner (1959) (ET59) and Briggs (1980) (B80).

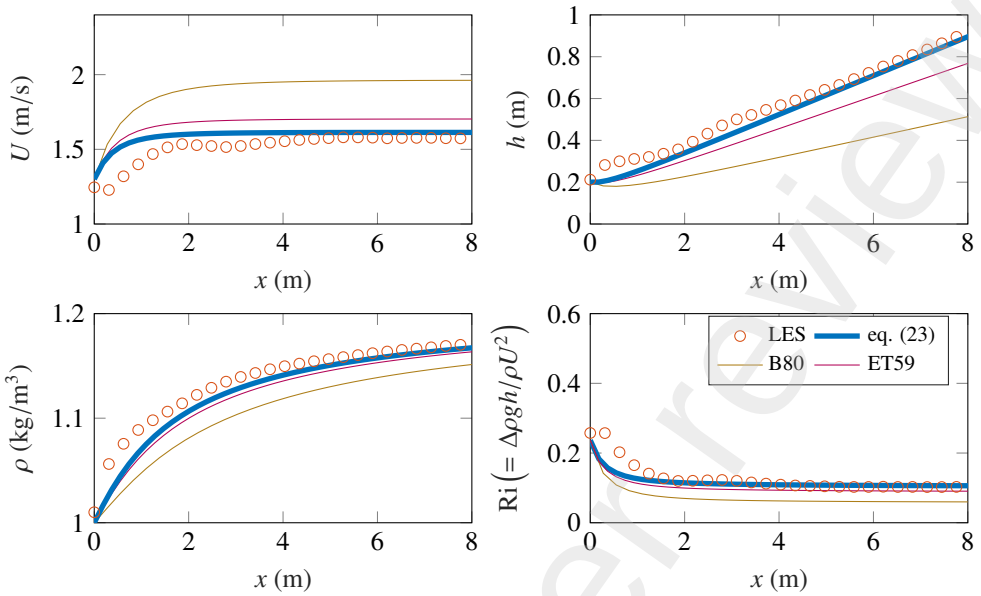

Figure 8: Evolution of the velocity, the height, the density and the Richardson number of the flow for the case 6 (θ = 77°). The red circles correspond to the LES simulation. The theoretical results are obtained by successively using the entrainment law given by equation (23) as well as the laws of Hopfinger (1983) based on the results of Ellison & Turner (1959) (ET59) and Briggs (1980) (B80).

line with its intended application for angles approaching 90°. Our law remains close to the LES simulation results, with an average relative error of 15% across the entire domain. Furthermore, this error is higher near the left boundary due to injection effects. Excluding this near-source region of limited spatial extent, the relative error decreases to below 10%.

Finally, and for illustrative purposes, we test the performance of our model in the planar wall plume configuration (i.e. with an angle of 90°). These results are presented in figure 9. The model provides a reliable prediction of the main variables (U, h and ρ) and the Richardson number, confirming its suitability even in this extreme configuration.

5. Conclusions

In this article, we investigated a miscible, steady, two-dimensional gravity current flowing along an inclined boundary. We focused on the evolution of its dynamics, of the entrainment coefficient E and on its dependence on both the slope and Richardson number.

To achieve this, we carried out eight large-eddy simulations, maintaining the injection conditions while varying the slope angle to cover a range from 0 to 90°. First, these simulations enabled us to observe the longitudinal evolution of the cross-section scales of velocity U, density ρ and height h of the current, as well as the Richardson number Ri, corresponding to the ratio between the buoyancy and inertial forces.

From these simulations, three distinct scenarios emerged. In the absence of slope (i.e., θ = 0°), the velocity and height exhibited a non-monotonic behaviour, with velocity decreasing initially, followed by an increase, and an opposite trend for the thickness. The Richardson

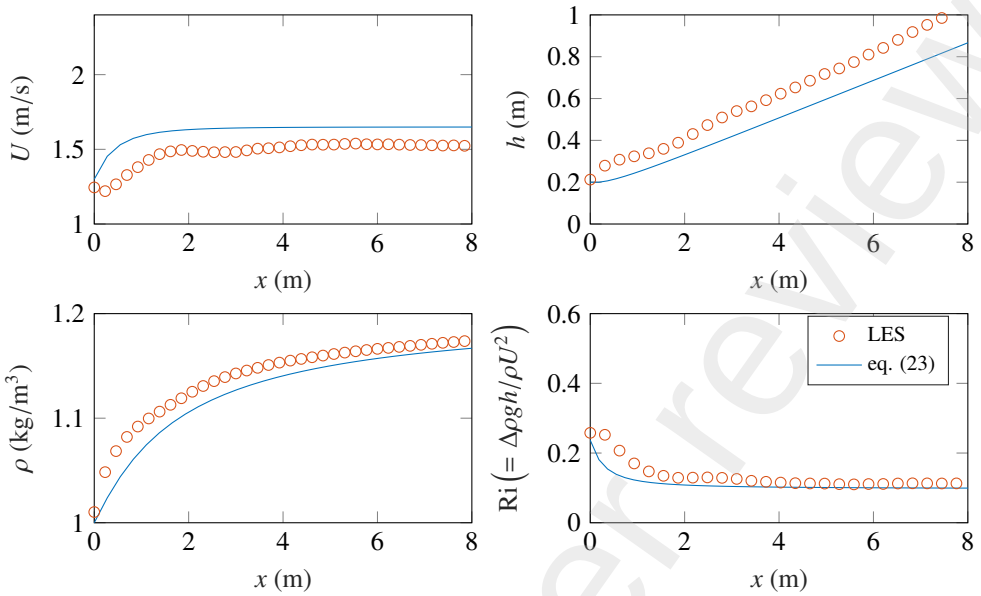

Figure 9: Evolution of the velocity, the height, the density and the Richardson number of the flow for the case 7 ($\theta = 90°$). The red circles correspond to the LES simulation and the blue lines corresponds to the model with the equation (23).

number displayed similar non-monotonic behaviour, increasing until it exceeds unity, then decreasing until the end of the domain. This indicated a flow transition from a supercritical to a subcritical regime. As the slope increased (between 5° and 35° according to our simulations), the flow showed a second regime characterized by an increasing Richardson number that stabilized at a value always below unity. In addition, both U and h displayed monotonic behavior, stabilizing toward the end of the domain. Finally, for angles exceeding 35°, we observed a third scenario in which the Richardson number decreased immediately after injection before stabilizing. In this configuration, the flow velocity increased from the injection point, gaining inertia in the streamwise direction.

Secondly, these simulations also enabled us to extract the local entrainment E. We noted a gradual increase of E with increasing slope angle, reaching a nearly constant value for a 90° angle. These findings are consistent with the existing literature for the two extreme cases ($\theta = 0°$ and $\theta = 90°$), with a dependence between the Richardson number and the entrainment for small angles and a constant entrainment coefficient for angles equal to or close to 90°. We develop a new entrainment model that includes both the influence of the Richardson number and the inclination. By combining the law of Christodoulou (1986) and data observed in the literature for a planar wall plume (Ellison & Turner (1959), Grella & Faeth (1975), Parker et al. (2020)), we proposed the law $E = 0.002\cos(\theta)/\mathrm{Ri} + 0.09\sin^{1/2}(\theta)$. This law unifies the entrainment of a gravity current with the entrainment of a planar wall plume.

In conjunction with the numerical study, we also examined the theoretical aspect of gravity currents. Our modeling was grounded in the work of Ellison & Turner (1959) and extended within the non-Boussinesq framework. This model, based on the equations of conservation of mass, momentum and buoyancy, allows the longitudinal evolution of velocity, thickness, density and Richardson number to be calculated. This model depends on the entrainment coefficient E

and exhibits a mathematical singularity when the Richardson number is equal to 1.

Following a mathematical analysis of the model, we analytically identified two specific angles: the critical angle θ_c and the supercritical angle θ_{sc}. The critical angle corresponds to the angle beyond which the mathematical singularity no longer exists. Consequently, for angles greater than θ_c, there is no mathematical difficulties in solving the equations. For its part, the supercritical θ_{sc} angle corresponds to the angle above which the Richardson number of the flow decreases immediately after the injection. In this configuration, the flow acquires inertia as it flows. These two angles were corroborated through LES simulations, with approximate values of 5° for θ_c and 35° for θ_{sc}.

Lastly, we employed our theoretical model with the proposed entrainment law and compared the results with those from models found in the literature. For each scenario identified (and illustrated respectively by the angles $\theta = 5°$, $\theta = 35°$ and $\theta = 77°$), our model provides better predictions than the laws from the literature. We also ran simulations at the two extreme cases, namely, 0° and 90° to confirm the model in the gravity current and in the planar wall plume configuration and the resolution of the theoretical model using the new entrainment law again provided results close to those obtained by LES simulation.

The newly developed entrainment law thus enhances the representativeness of the model proposed by Ellison & Turner (1959) across a range of angles from 0° to 90°. However, it is important to note that this model does not encompass all ranges of Richardson numbers. Specifically, the law presented by Christodoulou (1986) is only applicable for the range $\mathrm{Ri} \in [0.1, 10]$. For flows exhibiting more inertial or buoyant characteristics, it would be beneficial to modify the "gravity current" contribution of the entrainment law to ensure consistency with the existing literature.

6. Declaration of interests

The authors declare that they have no known competing financial interests or personal relationships that could have appeared to influence the work reported in this paper.

References

Ellison, T. & Turner, J., Turbulent entrainment in stratified flows. *Journal Of Fluid Mechanics*. **6**, 423-448 1959.

Griffiths, R., Gravity currents in rotating systems. *Annual Review Of Fluid Mechanics*. **18**, 59-89 1986.

Dufek, J., The fluid mechanics of pyroclastic density currents. *Annual Review Of Fluid Mechanics*. **48** pp. 459-485 2016.

Chowdhury, M. & Testik, F., Laboratory testing of mathematical models for high-concentration fluid mud turbidity currents. *Ocean Engineering*. **38**, 256-270 2011.

Hoult, D., Oil spreading on the sea. *Annual Review Of Fluid Mechanics*. **4**, 341-368 1972.

Alpert, R., Turbulent ceiling-jet induced by large-scale fires. *Combustion Science And Technology*. **11**, 197-213 1975.

Flynn, M. & Linden, P., Intrusive gravity currents. *Journal Of Fluid Mechanics*. **568** pp. 193-202 2006.

Turner, J., Turbulent entrainment: the development of the entrainment assumption, and its application to geophysical flows. *Journal Of Fluid Mechanics*. **173** pp. 431-471 1986.

Fernando, H., Turbulent mixing in stratified fluids. *Annual Review Of Fluid Mechanics*. **23**, 455-493 1991.

Lofquist, K., Flow and stress near an interface between stratified liquids. *The Physics Of Fluids*. **3**, 158-175 1960.

Princevac, M., Fernando, H. & Whiteman, C., Turbulent entrainment into natural gravity-driven flows. *Journal Of Fluid Mechanics*. **533** pp. 259-268 2005.

Jirka, G., Turbulent buoyant jets in shallow fluid layers. *Turbulent Buoyant Jets And Plumes*. pp. 69-119 1982.

Christodoulou, G., Interfacial mixing in stratified flows. *Journal Of Hydraulic Research*. **24**, 77-92 1986.

Wells, M., Cenedese, C. & Caulfield, C., The relationship between flux coefficient and entrainment ratio in density currents. *Journal Of Physical Oceanography*. **40**, 2713-2727 2010.

Cenedese, C. & Adduce, C., A new parameterization for entrainment in overflows. *Journal Of Physical Oceanography*. **40**, 1835-1850 2010.

Morton, B., Taylor, G. & Turner, J., Turbulent gravitational convection from maintained and instantaneous sources. *Proceedings Of The Royal Society Of London. Series A. Mathematical And Physical Sciences*. **234**, 1-23 1956.

Parker, G., Fukushima, Y. & Pantin, H., Self-accelerating turbidity currents. *Journal Of Fluid Mechanics*. **171** pp. 145-181 1986.

Johnson, C. & Hogg, A., Entraining gravity currents. *Journal Of Fluid Mechanics*. **731** pp. 477-508 2013.

Wells, M. & Wettlaufer, J., Two-dimensional density currents in a confined basin. *Geophysical & Astrophysical Fluid Dynamics*. **99**, 199-218 2005.

Britter, R. & Linden, P., The motion of the front of a gravity current travelling down an incline. *Journal Of Fluid Mechanics*. **99**, 531-543 1980.

Pawlak, G. & Armi, L., Mixing and entrainment in developing stratified currents. *Journal Of Fluid Mechanics*. **424** pp. 45-73 2000.

Pedersen, F., A monograph on turbulent entrainment and friction in two-layer stratified flow. Institute of Hydrodynamics 1980.

Briggs, G., Canopy effects on predicted drainage flow characteristics and comparisons with observations. *Bulletin of the American Meteorological Society*. **61**, 1501-1501 1980.

Hopfinger, E., Snow avalanche motion and related phenomena. *Annual Review Of Fluid Mechanics*. **15**, 47-76 1983.

Hughes, G. & Griffiths, R., A simple convective model of the global overturning circulation, including effects of entrainment into sinking regions. *Ocean Modelling*. **12**, 46-79 2006.

Salinas, J., Zuniga, S., Cantero, M., Shringarpure, M., Fedele, J., Hoyal, D. & Balachandar, S., Slope dependence of self-similar structure and entrainment in gravity currents. *Journal Of Fluid Mechanics*. **934** pp. R4 2022.

Grella, J. & Faeth, G., Measurements in a two-dimensional thermal plume along a vertical adiabatic wall. *Journal Of Fluid Mechanics*. **71**, 701-710 1975.

Parker, D., Burridge, H., Partridge, J. & Linden, P., A comparison of entrainment in turbulent line plumes adjacent to and distant from a vertical wall. *Journal Of Fluid Mechanics*. **882** pp. A4 2020.

Lai, M. & Faeth, G., Turbulence Structure of Vertical Adiabatic Wall Plumes. *Journal Of Heat Transfer*. **109**, 663-670, 1987.

Sangras, R., Dai, Z. & Faeth, G., Velocity statistics of plane self-preserving buoyant turbulent adiabatic wall plumes. *Journal of Heat Transfer*. **122**, 693-700 2000.

George, N., Ooi, A. & Philip, J., Evolution of a wall-attached buoyant plume in confined boxes: Direct numerical simulations, entrainment coefficient and an integral model. *International Journal Of Heat And Fluid Flow*. **90** pp. 108824 2021.

Haddad, S., Vaux, S., Varrall, K. & Vauquelin, O., Theoretical model of continuous inertial gravity currents including a jump condition. *Physical Review Fluids*. **7**, 084802 2022.

Haddad, S., Vaux, S., Varrall, K. & Vauquelin, O., Analytical solutions for long-time steady state Boussinesq gravity currents flowing along a horizontal boundary of finite length. *Physical Review Fluids*. **9**, 074803 2024.

Baines, P., Mixing in flows down gentle slopes into stratified environments. *Journal Of Fluid Mechanics*. **443** pp. 237-270 2001.

Baines, P., Mixing regimes for the flow of dense fluid down slopes into stratified environments. *Journal Of Fluid Mechanics*. **538** pp. 245-267 2005.

Nicoud, F. & Ducros, F., Subgrid-scale stress modelling based on the square of the velocity gradient tensor. *Flow, Turbulence And Combustion*. **62**, 183-200 1999

Bruneau, C. & Fabrie, P., Effective downstream boundary conditions for incompressible Navier–Stokes equations. *International Journal For Numerical Methods In Fluids*. **19**, 693-705 1994.

Bruneau, C. & Fabrie, P., New efficient boundary conditions for incompressible Navier-Stokes equations: a well-posedness result. *ESAIM: Mathematical Modelling And Numerical Analysis*. **30**, 815-840 1996.

Bruneau, C., Boundary conditions on artificial frontiers for incompressible and compressible Navier-Stokes equations. *ESAIM: Mathematical Modelling And Numerical Analysis*. **34**, 303-314 2000.

Zhou, X., Luo, K. & Williams, J., Large-eddy simulation of a turbulent forced plume. *European Journal Of Mechanics - B/Fluids*. **20**, 233-254 2001.

Kunsch, J., Critical velocity and range of a fire-gas plume in a ventilated tunnel. *Atmospheric Environment*. **33**, 13-24 1998.

Hu, L., Huo, R., Li, Y., Wang, H. & Chow, W., Full-scale burning tests on studying smoke temperature and velocity along a corridor. *Tunnelling And Underground Space Technology*. **20**, 223-229 2005.

Chow, W., Gao, Y., Zhao, J., Dang, J., Chow, C. & Miao, L., Smoke movement in tilted tunnel fires with longitudinal ventilation. *Fire Safety Journal*. **75** pp. 14-22 2015.

Chow, W., Gao, Y., Zhao, J., Dang, J. & Chow, C., A study on tilted tunnel fire under natural ventilation. *Fire Safety Journal*. **81** pp. 44-57 2016.

Henderson, F., Open Channel Flow. *Macmillan Publ. Company, N.Y.*. 1966.

Chanson, H., Hydraulics of open channel flow. (Elsevier) 2004.

Martin, A., Negretti, M., Ungarish, M. & Zemach, T., Propagation of a continuously supplied gravity current head down bottom slopes. *Physical Review Fluids*. **5**, 054801 2020.

Ungarish, M., Dam-break release of a gravity current in a stratified ambient. *European Journal Of Mechanics-B/Fluids*. **24**, 642-658 2005.

Nogueira, H., Adduce, C., Alves, E. & Franca, M., Analysis of lock-exchange gravity currents over smooth and rough beds. *Journal Of Hydraulic Research*. **51**, 417-431 2013

Rottman, J. & Simpson, J., Gravity currents produced by instantaneous releases of a heavy fluid in a rectangular channel. *Journal Of Fluid Mechanics*. **135** pp. 95-110 1983.

Monaghan, J., Meriaux, C., Huppert, H. & Monaghan, J., High Reynolds number gravity currents along V-shaped valleys. *European Journal Of Mechanics-B/Fluids*. **28**, 651-659 2009.

Shin, J., Dalziel, S. & Linden, P., Gravity currents produced by lock exchange. *Journal Of Fluid Mechanics*. **521** pp. 1-34 2004.

Sher, D. & Woods, A., Mixing in continuous gravity currents. *Journal Of Fluid Mechanics*. **818** pp. R4 2017.

Hogg, A. & Woods, A., The transition from inertia-to bottom-drag-dominated motion of turbulent gravity currents. *Journal Of Fluid Mechanics*. **449** pp. 201-224 2001.

Shringarpure, M., Lee, H., Ungarish, M. & Balachandar, S., Front conditions of high-Re gravity currents produced by constant and time-dependent influx: an analytical and numerical study. *European Journal Of Mechanics-B/Fluids*. **41** pp. 109-122 2013.

Zúñiga, S., Balachandar, S., Yang, Y., Zhang, Y., Smith, K., Loppi, N., Cantero, M. & Kerkemeier, S., Planar wall plumes bounded by vertical and inclined surfaces. *Physics Of Fluids*. **36** 2024.

Michaux, G. and Vauquelin, O. Solutions for turbulent buoyant plumes rising from circular sources. *Physics Of Fluids*. **20** 2008.

Vaux, S., Mehaddi, R., Vauquelin, O. & Candelier, F., Upward versus downward non-Boussinesq turbulent fountains. *Journal of Fluid Mechanics*. **867**, 374-391 2019.

Salizzoni, P., Vaux, S., Creyssels, M., Amielh, M., Pietri, L. & Anselmet, F., Turbulent transfer and entrainment in a low-density jet. *Journal of Fluid Mechanics*. **968**, A27 2023.

Salizzoni, P., Vaux, S., Creyssels, M., Craske, J.& van Reeuwijk, M., Entrainment in variable-density jets. *Journal of Fluid Mechanics*. **995**, A11 2024.